Astron. Astrophys. 356, 181–190 (2000)

ASTRONOMY AND ASTROPHYSICS

Evolution and surface abundances of red giants experiencing deep mixing

A. Weiss[1], **P.A. Denissenkov**[1,2], **and C. Charbonnel**[3]

[1] Max-Planck-Institut für Astrophysik, Karl-Schwarzschild-Strasse 1, 85748 Garching, Germany
[2] Astronomical Institute of the St. Petersburg University, Bibliotechnaja Pl. 2, Petrodvorets, 198904 St. Petersburg, Russia
[3] Observatoire Midi-Pyrénées, 14 Avenue Edouard Belin, 31400 Toulouse, France

Received 1 December 1999 / Accepted 11 February 2000

Abstract. We have calculated the evolution of low metallicity red giant stars under the assumption of deep mixing between the convective envelope and the hydrogen burning shell. We find that the extent of the observed abundance anomalies, and in particular the universal O-Na anticorrelation, can be totally explained by mixing which does not lead to significant helium enrichment of the envelope. On the other hand, models with extremely deep mixing and strong helium enrichment predict anomalies of sodium and oxygen, which are much larger than the observed ones. This latter result depends solely on the nucleosynthesis inside the hydrogen burning shell, but not on the details of the mixing descriptions. These, however, influence the evolution of surface abundances with brightness, which we compare with the limited observational material available. Our models allow, nevertheless, to infer details on the depth and speed of the mixing process in several clusters. Models with strong helium enrichment evolve to high luminosities and show an increased mass loss. However, under peculiar assumptions, red giants reach very high luminosities even without extreme helium mixing. Due to the consequently increased mass loss, such models could be candidates for blue horizontal branch stars, and, at the same time, would be consistent with the observed abundance anomalies.

Key words: stars: abundances – stars: evolution – stars: interiors – Galaxy: globular clusters: general

1. Introduction

The observed anomalies in CNO-, NeNa- and MgAl- elements in globular cluster red giants (see Kraft 1994 and Da Costa 1998 for reviews) are unexplained in canonical low-mass star evolution theory and indicate effects beyond the standard picture. At least for anomalies in those isotopes participating in the CNO-cycle models relying on the assumption of an additional, non-standard mixing process inside the stars have been presented, which explain convincingly the observations, including the evolution of the carbon abundance along the RGB, i.e. with time (see Charbonnel 1995; Denissenkov & Weiss 1996; Cavallo et al. 1998). This mixing is supposed to set in after the hydrogen burning shell has reached the composition discontinuity left behind by the first dredge-up on the red giant branch (RGB), i.e., after the so-called RGB bump (e.g. Sweigart & Mengel 1979; Charbonnel 1995; Charbonnel et al. 1998) where the molecular weight barrier between hydrogen burning shell and envelope is at a minimum. It is usually described in terms of a diffusion process of certain efficiency and penetration depth. The CNO anomalies and their correlations with brightness and metallicity (which are expected qualitatively from nucleosynthesis arguments in standard models, as discussed by Cavallo et al. 1998) are thus explained by a purely evolutionary picture (Smith & Tout 1992; Denissenkov & Weiss 1996; Boothroyd & Sackmann 1999a). The physical origin of the mixing process is believed to be found in differential rotation of the star and the parameters used in some of the presently available calculations have been derived from existing theories (e.g. Zahn 1992; Maeder & Zahn 1998), which are, however, far from being complete.

A similar situation holds for oxygen and sodium, which are found to be anti-correlated in globular cluster red giants (Kraft et al. 1993). Denissenkov & Denissenkova (1990) and Langer et al. (1993) showed that this could result from the mixing of elements participating in the ONeNa-cycle, which operates at higher temperatures than the CNO-cycle and therefore requires deeper mixing. Denissenkov & Weiss (1996) demonstrated how all anomalies of the mentioned elements known at that time can be explained by the deep mixing scenario. Their calculations were done by using canonical red giant models, which evolved along the RGB without any mixing, and performing the mixing and nuclear reactions in a post-processing way. For this approach to be correct it is necessary that the evolution of the background models is not affected by the mixing process. In fact, the mixing necessary to reproduce the observed anomalies was always so shallow that only very small amounts of hydrogen/helium were mixed between envelope and shell, even in the case of the O-Na-anti-correlation. This was taken as sufficient justification of the underlying basic assumption. Very similar conclusions were obtained by Cavallo et al. (1998).

Send offprint requests to: A. Weiss, (weiss@mpa-garching.mpg.de)
Correspondence to: A. Weiss

Within this approach, one cannot investigate the possibility or necessity for even deeper mixing, which would affect the hydrogen/helium structure of the models. Sweigart (1997a) has renewed the interest in such deep mixing by connecting the problem of horizontal branch morphology with that of observed anomalies, as previously suggested by Langer & Hoffman (1995). If the mixing leads to severe helium enhancement in the envelope, increased luminosities and stellar winds result, such that the star will populate the blue horizontal branch (HB), while it remains a red HB star without the additional mixing.

While Denissenkov & Weiss (1996) did not investigate the effect of helium transport, Sweigart (1997a) did not follow the evolution of the participating isotopes to compare with observations. In the present paper, we therefore attempt to close this gap by computing full evolutionary sequences which include deep diffusive mixing and by investigating abundance anomalies using these self-consistent models as background models. In particular, we want to answer the question *how much helium enrichment of the envelope is necessary or allowed to achieve or to keep consistency with observations.*

In Sect. 2 we will discuss the nucleosynthesis aspects of the problem and review the observational status of the global O-Na anticorrelation, which is a powerful tracer of the transport processes in the red giants. In Sect. 3 we will present and discuss the evolutionary models. After that, the predictions for the abundances based on our mixed models and post-processing nucleosynthesis will follow, before the conclusions close the paper.

2. The O-Na anticorrelation: Observational status and nucleosynthesis arguments

Among the chemical anomalies observed in red giant atmospheres over the past two decades, the variations in oxygen and sodium have a special status. Indeed, the so-called global oxygen-sodium anticorrelation appears to be a common feature to all the globular clusters in a wide range of metallicity (-2.5≤[Fe/H]≤-1), for which detailed abundance analysis of the brightest giants have been carried out (Gratton & Ortolani 1989; Sneden et al. 1991; Drake et al. 1992; Brown & Wallerstein 1992; Kraft et al. 1993; Armosky et al. 1994; Minniti et al. 1996; Pilachowski et al. 1996; Kraft et al. 1997; Kraft et al. 1998). This pattern shows up in "normal" monometallic clusters (M3, M4, M5, M10, M13, M15, M92, NGC 7002) as well as in the multi-metallicity cluster ω Cen (Paltoglou & Norris 1989; Norris & Costa 1995). Fig. 1 summarizes the present observational status concerning the O-Na-anticorrelation. But more importantly, this feature, and the dependence of the Na enhancement and O depletion on the red giant evolutionary state (Pilachowski et al. 1996; Kraft et al. 1997) can be explained straightforwardly in the deep mixing scenario (Denissenkov & Weiss 1996).

Regarding the Mg and Al anomalies, the situation is very different, and the observed Mg-Al anticorrelation (Shetrone 1996a) requires a combination of the deep

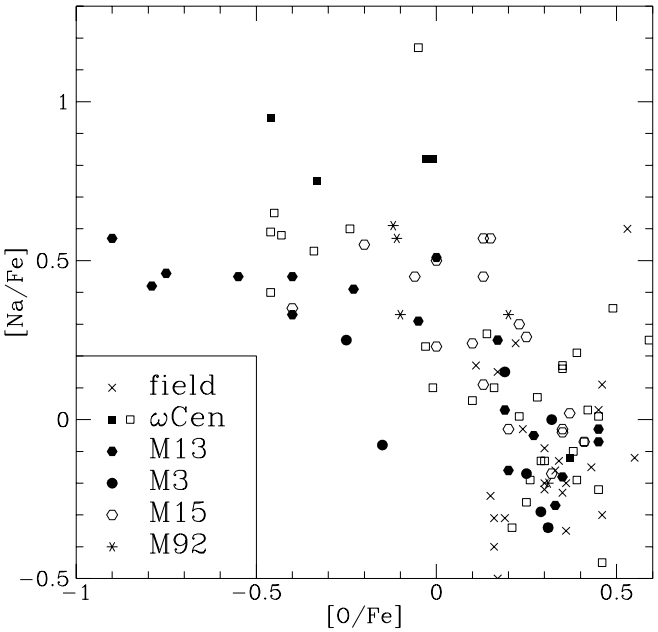

Fig. 1. Observed [Na/Fe] vs. [O/Fe] for galactic globular cluster and field giants. References for the data are: Field: Shetrone (1996a), Shetrone (1996b), M3: Kraft et al. (1992), M13: Kraft et al. (1997), M15: Sneden et al. (1997), M92: Shetrone (1996a), ω Cen: Norris & Costa (1995). In ω Cen, black and white squares correspond to stars with [Fe/H] higher and lower than -1, respectively

mixing and primordial scenarios (Denissenkov et al. 1997; Denissenkov et al. 1998). *Ad hoc* assumptions would be needed to obtain the observed ^{24}Mg depletion within the low mass Al-rich giants themselves (Shetrone 1996b). Since a low energy resonance in the ^{24}Mg(p,γ)^{25}Al reaction remains undetected (Angulo et al. 1999) or even can be excluded (Powell 1999), "exotic" models are required to episodically increase the temperature of the hydrogen-burning shell up to values as high as $\sim$ 70-85 MK (while canonical models reach a maximum temperature of only 55 MK) in order to deplete Mg at the expense of ^{24}Mg (Langer et al. 1997; Zaidins & Langer 1997; Fujimoto et al. 1999) inside the low mass giants as apparently being the consequence of the results by Shetrone (1996a and 1996b) for M13. Lately, however, Ivans et al. (1999) found that Mg and Al abundance variations in M4 can be explained completely by the idea that the Al-enhancement is due to a destruction of the Mg-isotopes ^{25}Mg and ^{26}Mg (cf. Fig. 2). Even in this case, a significant increase of the initial abundance of ^{25}Mg is required (Denissenkov et al. 1998). Since the Mg-Al anticorrelation cannot be explained by the deep mixing scenario alone, we do not consider it further in this paper. In fact, all explanations brought forward up to now being rather exotic and complicated, one should also wait for additional observational support for its existence (as well as for the isotopic ratios) and relation to other stellar properties before advocating any explanations.

Last but not least, the morphology of the global O-Na anticorrelation (Fig. 1) bears crucial clues on the mixing process. First, its extension to very low oxygen abundances ([O/Fe] ≤ -0.45) is entirely due to the contribution of M13 red giants. It

is this "second parameter" globular cluster that has the fastest rotating blue horizontal branch (HB) stars. Peterson et al. (1995) found six stars having $v \sin i \geq 30$ km s^{-1}. In the same paper red HB stars in M3 (the cluster forming a classical "second parameter"-pair with M13) have been found to possess smaller projected rotational velocities, from 2 to 20 km s^{-1}. This indicates a relation between rotation and mixing.

Concerning this extension along the horizontal axis, our experience in modelling the global anticorrelation shows that it depends primarily on the mixing rate $D_{\rm mix}$ or, more precisely, on the product "mixing rate $\times$ mixing time". We will come back to these arguments in Sect. 4, where our nucleosynthesis predictions in deeply mixed stars will be compared to the observations of [O/Fe] versus [Na/Fe].

Secondly, the extension of the global anticorrelation along the vertical axis ($-0.4 \leq$ [Na/Fe] ≤ 0.6 in all clusters except ω Cen) tells us mostly about the depth of the additional mixing. In Denissenkov & Weiss (1996, Fig. 4) and in Denissenkov et al. (1998, Fig. 1) it has been shown that on approaching the hydrogen burning shell the Na abundance displays two successive rises (see Fig. 2). The first rise results from the reaction ^{22}Ne(p,γ)^{23}Na, whereas the deeper one is produced in the NeNa-cycle by the partial consumption of ^{20}Ne, which is much more abundant than both ^{22}Ne and ^{23}Na. The size of the vertical extension of the global anticorrelation implies that additional mixing, whatever it is, does not penetrate the second step (rise) in the Na abundance profile where H starts to decrease. Otherwise, observed [Na/Fe] values would be much larger than they are[1]. Cavallo et al. (1998) have investigated the dependence of the abundance profiles on metallicity (and mass). Their results confirm our arguments completely. Only for stars of near-solar metallicity very deep mixing with significant helium enrichment but without strong sodium enhancement could be possible (see also Fig. 5 of Denissenkov & Weiss 1996). However, the clusters under discussion (e.g. M13) are metal-poor. Let us note in Fig. 1 the different behavior of field stars (Shetrone 1996a, Shetrone 1996b). In this population, the O-Na-anticorrelation is not present (Gratton et al. 2000). This indicates that the deep mixing does not penetrate the region where ON-burning occurs, and may reveal possible environmental effects on its efficiency.

To prepare Fig. 2 we applied a nucleosynthesis code to a red giant model with surface luminosity $\log L/L_\odot = 2.21$ from which our nucleosynthesis with additional deep mixing calculations started (Sect. 3). The considerable growth of the ^{27}Al abundance with depth is due to our "non-standard" assumption of an enhanced initial abundance of the ^{25}Mg isotope ([^{25}Mg/Fe] $= 1.1$) and of the thousandfold enhanced rate of the reaction ^{26}Al$^{\rm g}(p,\gamma)^{27}$Si (for details see Denissenkov et al. 1998). These ad hoc modifications were needed to explain the observed Al enhancements (Denissenkov et al. 1998), but have no influence

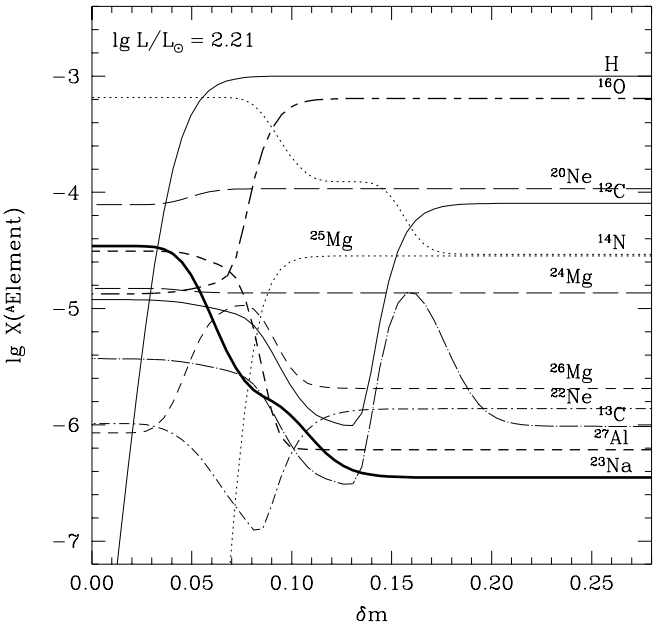

Fig. 2. Abundances of some isotopes participating in the CNO-, NeNa- and MgAl-cycle as functions of the relative mass coordinate ($\delta m = 0$ at the bottom of the hydrogen burning shell and $\delta m = 1$ at the bottom of the convective envelope) in the red giant model from which detailed nucleosynthesis calculations with extra mixing start. ^{23}Na is emphasized by a thick solid line. Also shown is the hydrogen abundance profile, normalized, however, to 10^{-3} to accommodate it on the same scale

on the results of the present paper. From Fig. 2, we see immediately that if extra mixing penetrates down to layers, say, at $\delta m \approx 0.06$, this will result in an enrichment of the red giant's envelope in N, Na and Al and in its impoverishment in C, O, and ^{25}Mg. Again, ^{24}Mg remains unchanged due to the relatively low temperatures reached in such a star. These results were recently confirmed by Palacios et al. (1999) in models using the reaction rates recommended by NACRE (Angulo et al. 1999).

3. Red giant evolution with deep mixing

To produce background models for the nucleosynthesis post-processing we have evolved stellar models under the assumption of additional deep mixing after the RGB bump. All sequences were started at the same initial model, which consisted of an $0.8\,M_\odot$ star of initial composition $Y = 0.25$ and $Z = 0.0003$, and which had been evolved (canonically) up to the luminosity of the bump, i.e., $\log L/L_\odot = 2.21$ (at this point, its mass is $0.798\,M_\odot$). The envelope helium content has increased to 0.256 (in mass fraction) due to the first dredge-up. The input physics of the Garching stellar evolution code (used here) is up-to-date (for a summary, see Denissenkov et al. 1998), but atomic diffusion has not been included in the computations.

The additional deep mixing between the convective envelope and some point inside the hydrogen shell has been implemented in the same general line as in our previous papers on this subject, that is, as a diffusive process with parameterized values for the diffusive constant $D_{\rm mix}$, which is the same for

[1] Actually some metal-rich giants in ω Cen show extremely high [Na/Fe] (up to 1 dex), probably indicating a penetration of the mixing to the second rise of Na. This cluster is the only one where some giants exhibit surface enrichment of Na produced from both ^{20}Ne and ^{22}Ne. It also has one of the bluest horizontal branches (Whitney et al. 1994).

all elements, and for the penetration depth. The values used for $D_{\rm mix}$ are guided by the results of our earlier papers, and agree with estimates based on rotationally induced mixing theories. We refer the reader to Denissenkov & Weiss (1996) for details of this approach. We use the normalized mass coordinate δm introduced therein, which is 0 at the bottom of the hydrogen shell (usually, where $X = 10^{-4}$) and 1 at the bottom of the convective envelope. The choice of this mass coordinate allows accurate interpolation between a small number of background models in the nucleosynthesis calculations (see Cavallo et al. 1998 for a similar approach). The shell, in this coordinate, is located below $\delta m \approx 0.10$. The depth, down to which the diffusive mixing should occur, we denote as $\delta m_{\rm mix}$. Obviously, due to the lack of solid theories, one could also choose, for example, purely geometrical scales to define the penetration depth (Boothroyd & Sackmann 1999b). Contrary to our earlier papers, the criterion for penetration is not determined by a fixed value for $\delta m_{\rm mix}$ chosen before the calculations, but is related to the decrease in hydrogen content within the shell (relative to the surface or convective envelope abundance $X_{\rm env}$), expressed as a free parameter $\triangle X$. We have investigated several different prescriptions for the penetration criteria and found a great sensitivity of the mixing on these prescriptions, which are

1. find that $\delta m_{\rm mix}$ in the initial model, where $X = X_{\rm env} - \triangle X$, and mix to the same $\delta m_{\rm mix}$ in all subsequent models;
2. as 1., but $\delta m = 0$ is defined as the point where $X = X_{\rm env}/2$ (instead of $X = 10^{-4}$);
3. as 1., but the diffusion constant $D_{\rm mix}$ is decreasing exponentially from the maximum value D_0 for $\delta m > 0.10$ to $D_{\rm mix} \approx 5 \cdot 10^{-5} D_0$ at $\delta m_{\rm mix}$
4. always mix to the point, where $X = X_{\rm env} - \triangle X$

Except for method 3, these schemes were chosen to be as simple as possible and to be similar to the one by Sweigart (1997a).

Keeping the relative mass coordinate fixed, up to which mixing should occur, implies that changes in the hydrogen profile in the shell (usually steepening in the course of evolution) or in the extend of the convective envelope influence the mixing. As an illustration of the "movement" of the profile in this coordinate we display in Fig. 3 an example ($D_{\rm mix} = 10^9\,{\rm cm^2\,s^{-1}}$; $\triangle X = 0.20$; method 1). The smooth solid line is the initial model. The next model (at $\log L/L_\odot = 2.288$) is the leftmost line. From there, the model profiles shift to the right again. The solid line with clearly reduced hydrogen abundance throughout the envelope corresponds to a model close to the RGB-tip ($\log L/L_\odot = 3.539$). In this phase the burning time at the bottom of the mixed region becomes short enough to lead to "bottom-burning" of the envelope. An extended RGB-phase with luminosities drastically increased above the canonical RGB-tip luminosity of $\log L_{\rm tip}/L_\odot = 3.33$ is the result; the final value being $\log L_{\rm tip}/L_\odot = 3.8$. Since mass loss (Reimers 1975, with $\eta = 0.3$) was taken into account, the total mass at the tip decreases in such cases below $0.6\,M_\odot$. $\delta m_{\rm mix}$ is indicated by the vertical line and is 0.047.

Using method 2 instead, $\delta m = 0$ is defined as the point where the abundance of hydrogen has dropped to half the surface value of the same model ($\delta m_{\rm mix} = 0.0066$ in this case). This prevents, obviously, any penetration to shell regions with lower hydrogen content. As in the previous case, the bottom of the envelope is burnt at the end of the RGB evolution. However, as soon as the hydrogen abundance approaches $X_{\rm env}/2$ (guaranteed as long as mixing is not quasi-instantaneous), the mixing criterion inhibits further mixing. For this reason X remains constant for $\delta m < 0$; in the final models $X_{\rm env} = 0.6402$ and the hydrogen profile always has a finite step in the shell. In this case, the luminosity rises to $\log L_{\rm tip}/L_\odot = 3.53$.

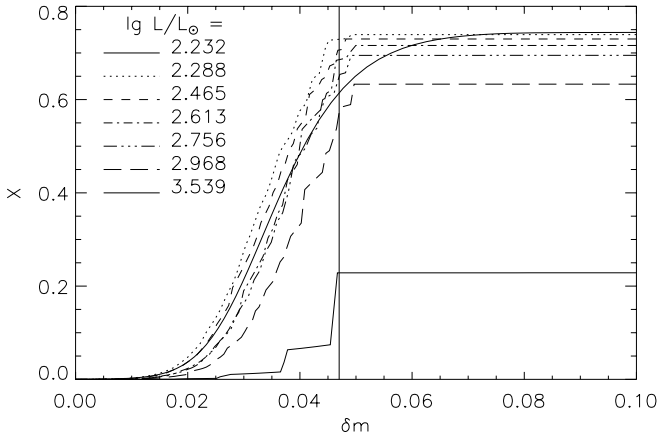

Fig. 3. Hydrogen profiles in the normalized δm coordinate in models with deep mixing during the evolution along the RGB. Mixing parameters were $D_{\rm mix} = 10^9\,{\rm cm^2\,s^{-1}}$; $\triangle X = 0.20$, method 1. The vertical line is the mixing depth $\delta m_{\rm mix}$ as defined in the first model. See text for more explanations

The steps visible in the chemical profiles of Fig. 3 are due to the diffusion criterion applied to the numerical grid, because no interpolation to the exact value of $\delta m_{\rm mix}$ had been done. We verified that the results do not depend on the grid resolution, which was increased by a factor of 10 in the shell in part of the calculations. Only the steps got smaller and more numerous. To avoid such steps, we introduced a varying diffusion constant (method 3) motivated by recent results of Denissenkov & Tout (2000). They have proposed a physical mechanism for extra mixing in red giants which quantitatively interprets all the known star-to-star abundance variations in globular clusters. This is Zahn's mechanism (Zahn 1992; Maeder & Zahn 1998) which considers extra mixing in a radiative zone of a rotating star as a result of the joint operation of meridional circulation and turbulent diffusion. This process was already advocated by Charbonnel (1995) to explain the low carbon isotopic ratios and lithium abundances in field Population II giants and to lower the ^{3}He yields by low mass stars. Denissenkov & Tout report that the mixing rate does not vanish abruptly at a particular depth but instead it dies out gradually on a rather short depth range approximately between $\delta m = 0.10$ and $\delta m = 0.06 \sim 0.07$. This explains the following choice of an exponential decline approach for $D_{\rm mix}$:

$$D_{\rm mix} = D_0;\ \delta m > \delta m_0$$
$$= D_0 \exp\left[c_D \left(\frac{\delta m_0 - \delta m}{\delta m_{\rm mix} - \delta m_0}\right)\right];\ 0 \le \delta m \le \delta m_0 \quad (1)$$

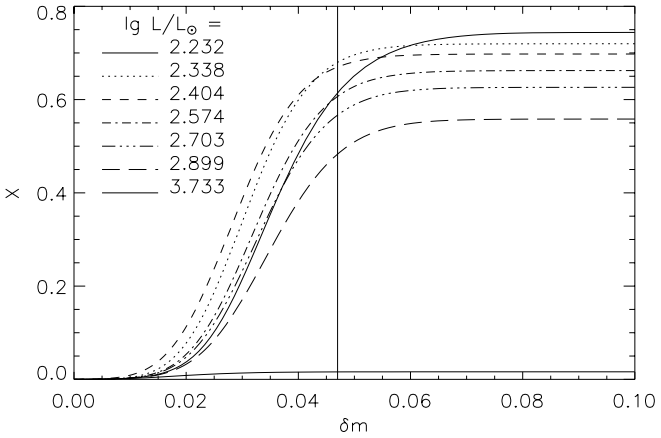

Fig. 4. As Fig. 3, but for an exponentially declining diffusion coefficient $D_{\rm mix}$ (Eq. 1). The results shown are from case D in Table 1

Table 1. Parameters of calculations presented in Figs. 5–7 and final values of the stellar mass ($M_{\rm f}/M_\odot$) and luminosity ($\log L_{\rm f}/L_\odot$), and of the helium mass fraction in the envelope ($Y_{\rm env}$). The final luminosity $L_{\rm f}$ is always very close or identical to the RGB-tip luminosity $L_{\rm tip}$. The mass loss in sequences B and C' has been reduced by a factor 20 compared to the other ones. The penetration depths, expressed in the normalized mass coordinate δm corresponding to the three $\triangle X$ values are 0.060 (0.05), 0.054 (0.10), and 0.047 (0.20). $D_{\rm mix}$ is in units of $\rm cm^2\,s^{-1}$

case	$D_{\rm mix}$	$\triangle X$	method	$M_{\rm f}$	$Y_{\rm env}$	$\log L_{\rm f}$
S	0.0	—	—	0.689	0.256	3.31
A	$5\cdot10^8$	0.05	3	0.586	0.270	3.79
B	$5\cdot10^8$	0.10	2	0.792	0.284	3.30
C	10^9	0.20	2	0.567	0.360	3.53
C'	10^9	0.20	2	0.771	0.360	3.56
D	10^9	0.20	3	0.562	0.351	3.77

where $\delta m_0 = 0.10$ was used for the beginning of the decline and $\delta m_{\rm mix}$ is the mixing depth coordinate as defined in method 1. Using $c_D = 10$ ensures that $D_{\rm mix}(\delta m_{\rm mix}) \approx 5\cdot10^{-5}D_0$. The resulting evolution (Fig. 4) is similar to that of the case shown in Fig. 3, but the profiles are smooth; mixing parameters are identical.

We finally note that method 4, applied straightforwardly, leads to a complete burning of the entire envelope for $D_{\rm mix} \geq 5\cdot10^8$ and/or $\triangle X \geq 0.10$. However, this we consider to be an artefact, which is easy to understand: Since due to the mixing the hydrogen abundance in the envelope is reduced, the critical point down to which mixing should occur, is moving inwards. Therefore layers of even lower hydrogen content are mixed with the envelope, and the critical point moves to even deeper regions. Only at the point where the burning time-scale is shorter than the mixing time-scale and therefore the surface hydrogen content no longer is able to adjust to the burning, this process is stopped. A way out of this situation is to ensure that the mixing does not lead to a sharp step in the shell's hydrogen profile. This way, the critical point can be kept within the mixed layers. While the mixing procedure described in Sweigart (1997a) appears to follow the straightforward approach, Sweigart (private communication, 1999) in fact used a more complicated method to keep the hydrogen profile even in the presence of mixing. Our method 3 qualitatively has the same effect.

To summarize, method 4 appears to be unphysical; method 3 is based on the physical picture by Denissenkov & Tout (2000), but makes additional parameters necessary. Methods 1 and 2 are the most straightforward choices leading to composition profiles similar to method 3; method 2 differs from 1 in that it avoids complete mixing and burning of the envelope during the very last phases of RGB evolution.

Obviously the details of the mixing procedure influence the resulting evolution to quite a significant extent. Since at present we are far from providing a solid physical approach (which could allow, for example, for a diffusion speed varying both in space and time), we cannot predict the true evolution of a star experiencing deep mixing. However, the calculations are needed only to provide background models with varying degrees of helium mixing into the envelope, and it is of no importance how this is achieved in detail. We have calculated 25 different sequences, varying method and parameters. The cases selected for Table 1 are representative for the range of results we obtained, which are summarized in Figs. 5, 6, and 7. Case D of Table 1 is the one also shown in Fig. 4. We add that the amount of mass loss has no influence on the mixing properties. Neither does a gradual switching-on of the additional mixing during the first few models. We have performed some comparison calculations with a completely different code (the Toulouse-Geneva code; Charbonnel et al. 1992). While the results differ in details, the gross properties are the same. The differences we ascribe to details in the mixing procedures and the implementation of diffusion.

The effects on the evolution, displayed in Figs. 5 – 7, are qualitatively as expected from the work by Sweigart (1997a). The increase in the surface helium content is quite dramatic in cases C and D (fast and very deep mixing). However, it is not as large as in Sweigart (1997a), shown, for example, in his Fig. 2, where for $\triangle X = 0.20$ a value of $Y \gtrsim 0.42$ was reached. Also, in contrast to Sweigart's result, in all our calculations the helium enrichment of the outer envelope tends to level off with progressing evolution. This might be ascribed again to differences in the mixing scheme details, as we find these differences also in the post-processing models presented in the next section (cf. Figs. 10 and 12). We also find that the luminosities can get extremely high (cases A and D) with high mass loss as the consequence and a beginning turn-away from the RGB before the He-flash sets in. The beginning of such an evolution might be recognised, too, in Fig. 3 of Sweigart (1997b) in the case of deepest mixing. We also note that mixing method 2 (cases B and C) results in loops in the HRD, which depend on the occurrence of mixing episodes. This is, for example, visible in the non-monotonic luminosity evolution in Fig. 6.

The lifetime on the RGB is in all cases prolonged (Fig. 7) by 1 or 2 Myr, in some cases up to 4 Myr (5–10% of the lifetime after the bump). The evolutionary speed is influenced mainly

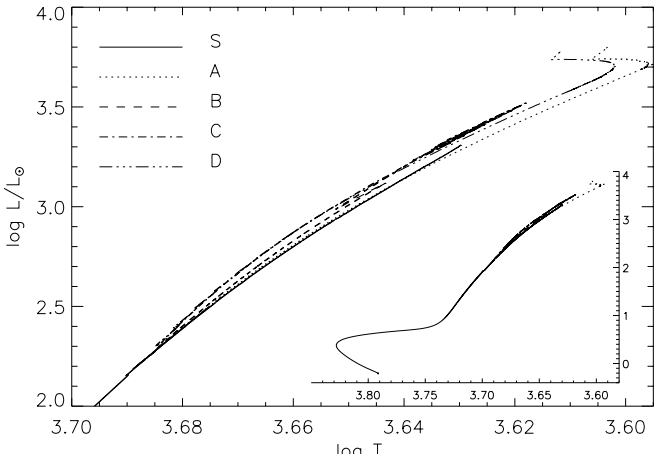

Fig. 5. HRD of four mixed sequences of Table 1 and the unmixed canonical one (S) for comparison. The linetypes refer to the cases listed in Table 1 and are given in the top-left corner. The large plot shows the upper RGB evolution only, the inset the complete evolution from the ZAMS on.

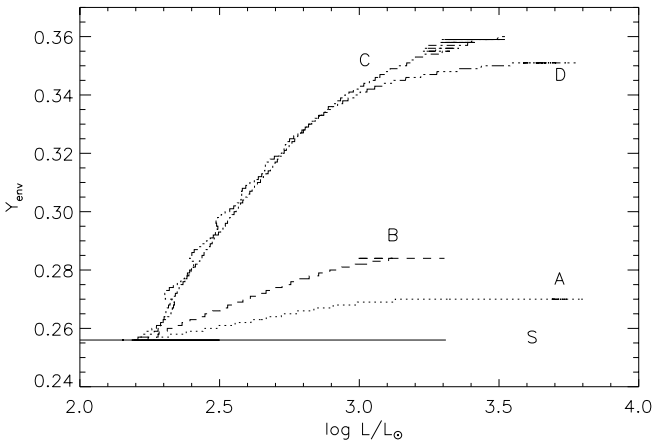

Fig. 6. Surface helium abundance (in mass fraction) as a function of luminosity for the same sequences as in Fig. 5. A coarseness of 0.001 is due to the limited number of digits in the output

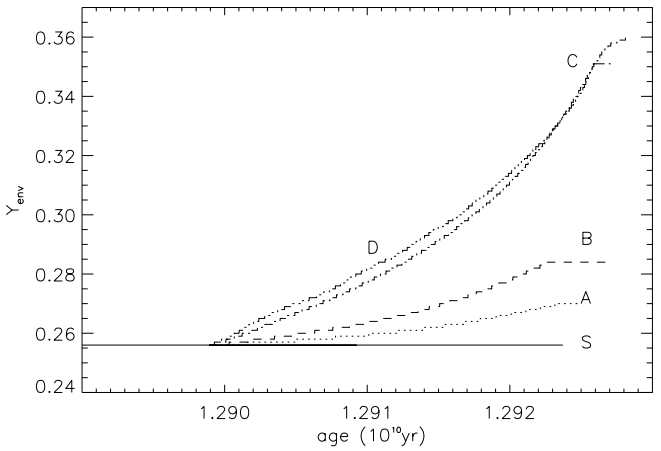

Fig. 7. Surface helium abundance as a function of age for the same sequences as in Fig. 5

immediately after the onset of the additional mixing (after the bump). From the initial model to one at $\log L/L_\odot \approx 2.5$, the time increases from 7 Myr (case S) to about 10 Myr (A & B) and 13 Myr (C & D). Thereafter, it is becoming comparable again in all cases. Such an effect could possibly be seen in luminosity functions, but it should be most prominent only in a limited luminosity range. VandenBerg et al. (1998) have argued that the luminosity function of M30 could be evidence for rapidly rotating cores of giants.

In some calculations, in particular those employing the exponentially declining diffusive speed (method 3), an interesting effect appeared. Although the mixing for moderate penetration depth and mixing speed remains small, the luminosity of the models rises to extreme values. As an example, in case A ($\triangle X = 0.05$, $D_{\rm mix} = 5 \cdot 10^8\,{\rm cm^2\,s^{-1}}$), $Y_{\rm env} = 0.270$ (an enrichment of only $+0.014$) and $\log L/L_\odot = 3.79$ were reached at the tip of the RGB (see also Fig. 5). An inspection of the models shows that part of the extended region of almost homogeneous composition, which is achieved due to the effect of the additional diffusion, becomes hot enough for significant hydrogen burning. In Fig. 8 we display the H-profiles of selected models in this phase. The first one (top line) is at $\log L/L_\odot = 2.73$ ($Y_{\rm env} = 0.265$). In this model, the point were the energy production due to hydrogen burning exceeds $10^3\,{\rm erg\,g^{-1}\,sec^{-1}}$ for the first time, is very close to the composition step. In the next model ($\log L/L_\odot = 3.12$; $Y_{\rm env} = 0.269$) this point has shifted to $\delta m = 0.274$ and is constantly progressing outward until it reaches $\delta m = 0.80$ in the most advanced models at the bottom of the figure ($\log L/L_\odot = 3.68$; $Y_{\rm env} = 0.270$). This burning of the plateau constitutes a broadening of the hydrogen shell and delivers extra luminosities. In fact, 50% of the total luminosity of the models with the plateau value around $X = 0.40$ are generated at $\delta m > 0.06$, that is outside the inner composition step. Therefore, the luminosity in excess of that of an ordinary star at the tip of the RGB (around $\log L/L_\odot = 3.30$) can completely be ascribed to the plateau burning (note that diffusion cannot keep the burning plateau homogeneous with the outer regions). The effect we observe here is probably due to our mixing description, which sets $D_{\rm mix}$ to the maximum value outside $\delta m = 0.10$. If our mixing description is realistic, this would imply that one could get very high luminosities at the RGB-tip *without* extreme helium mixing. The time spent at luminosities above the standard TRGB brightness is only 10^6 yrs and therefore observation of such a superluminous star is rather unlikely. Due to the extreme overluminosities, the Reimers mass loss formula leads to stellar winds of order $10^{-7}\,M_\odot$/yr and a final mass of $0.58\,M_\odot$ ($M_c = 0.517\,M_\odot$). After the helium flash, this star will populate the blue part of the horizontal branch.

4. Nucleosynthesis in deeply mixed stars

The detailed nucleosynthesis calculations we present now have been performed in a post-processing way as in our previous works (Denissenkov & Weiss 1996; Denissenkov et al. 1998). From an evolutionary sequence three red giant models were

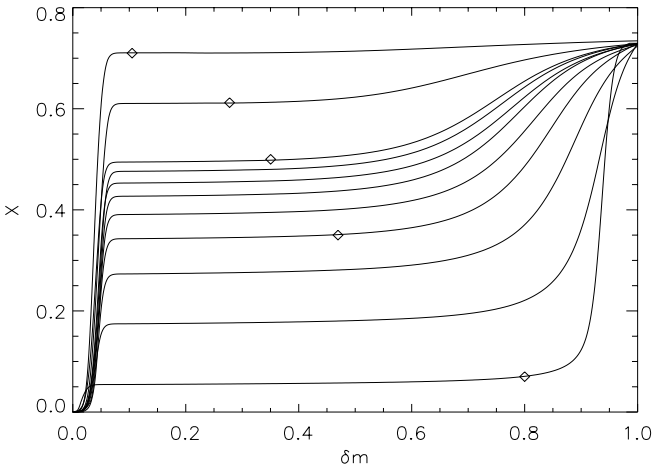

Fig. 8. Hydrogen profiles of selected models at the tip of sequence A ($\triangle X = 0.05$, $D_{\rm mix} = 5 \cdot 10^8\,{\rm cm^2\,s^{-1}}$, mixing method 3). The point where energy generation by hydrogen burning exceeds $10^3\,{\rm erg/(gs)}$ first, is indicated in several models by symbols.

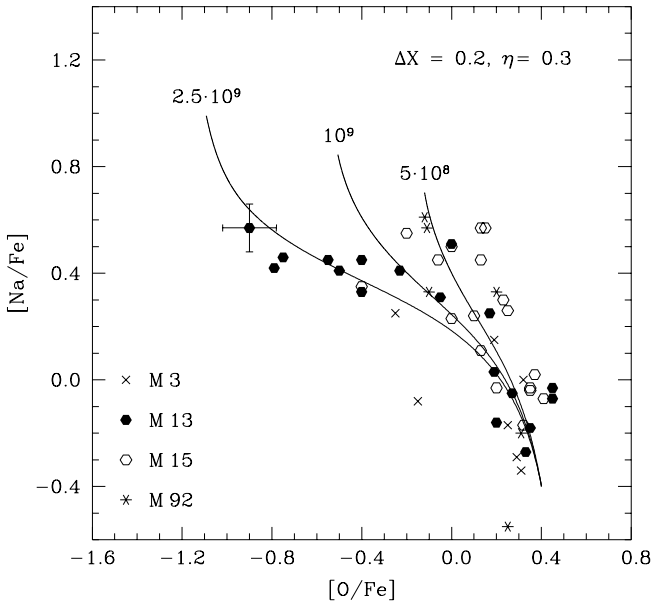

Fig. 9. The global anticorrelation and three theoretical curves (labelled by the value of $D_{\rm mix}$ used in the corresponding calculation); all three curves were calculated with the penetration criterion 1 and $\triangle X = 0.2$; *unmixed* red giant models were used as background. Observational data (omitting $\omega\ Cen$) are as in Fig. 1

selected. The starting one was the same one as for the full evolutionary calculations discussed in the previous section, i.e. a model at the bump ($\log L/L_\odot \approx 2.2$) in which the hydrogen burning shell had recently crossed the H-He discontinuity left by the base of the convective envelope on the first dredge-up phase. The final one was a model near the RGB tip ($\log L/L_\odot \approx 3.3$), the second one having a luminosity intermediate to those of the starting and finishing models. Distributions of T, ρ and r with δm in these three "background" models were used for interpolations in $\log\ L$ during the nucleosynthesis calculations. Further details about our post-processing procedure can be found in Denissenkov & Weiss (1996). The network of nuclear kinetics equations was the smallest one of those considered in Denissenkov et al. (1998). It takes into account 26 particles coupled by 30 nuclear reactions from the pp-chains, CNO-, NeNa- and MgAl-cycle. The additional mixing is modelled by diffusion with a constant coefficient $D_{\rm mix}$. We recall that we allow for mixing prescriptions and parameters in these calculations different from those for which the background models have been obtained.

For the comparison with observations we have preferred the "global anticorrelation" of [O/Fe] versus [Na/Fe] for the reasons detailed in Sect. 2. In Fig. 9 and Fig. 11 it is plotted for globular clusters according to the latest observational data.

In Fig. 9 theoretical dependences of [Na/Fe] on [O/Fe] obtained in the post-processing way for three values of the diffusion coefficient are shown. This first set of calculations was performed with *unmixed* background red giant models like in our previous papers but with mass loss taken into account. The depth of additional mixing was determined according to the penetration criterion 1 (Sect. 2) with $\triangle X = 0.2$. The mass loss rate $\dot{M}$ was estimated with Reimers (1975) formula in which the parameter value $\eta = 0.3$ was adopted. In Fig. 10 the resulting envelope He abundances are shown as functions of $\log\ L/L_\odot$. The mixing depth in the starting model which was kept constant

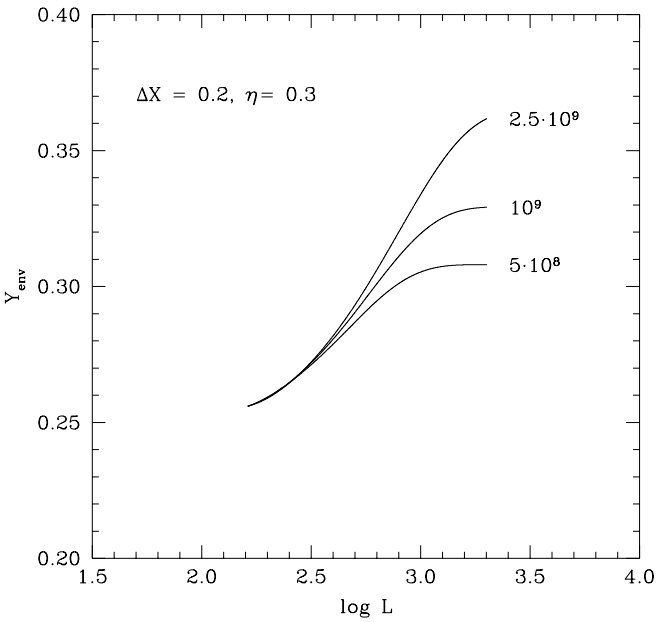

Fig. 10. The same three curves as in Fig. 9 in the $\log\ L$ - $Y_{\rm env}$ plane

during the nucleosynthesis calculations was $\delta m_{\rm mix} = 0.047$. Such a value of $\delta m_{\rm mix}$ allows some (modest) penetration of the second Na step (see Sect. 2) by the mixing which results in an upward steepening of the theoretical dependences of [Na/Fe] on [O/Fe] by the end of the RGB evolution (Fig. 9). The maximum He enrichment achieved in the envelope in this set of calculations is $\triangle Y_{\rm env} \approx 0.10$ (Fig. 10).

In the next nucleosynthesis calculations, the results of which are presented in Figs. 11 and 12, we have used *mixed* background

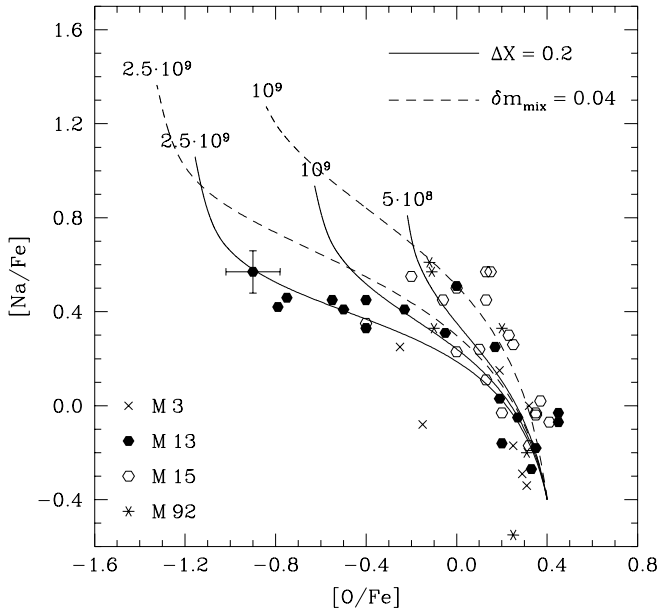

Fig. 11. As Fig. 9, but for calculations using *mixed* red giant models as background. The solid curves were calculated with the penetration criterion 1 and $\triangle X = 0.2$ and the dashed ones with constant mixing depth $\delta m_{\rm mix} = 0.04$

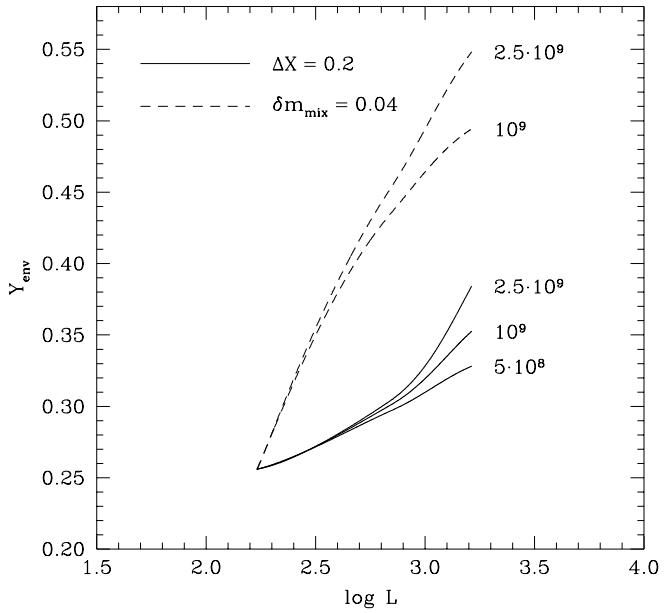

Fig. 12. The same five curves as in Fig. 11 in the $\log L$ - $Y_{\rm env}$ plane

models from sequence C' of Table 1; for this sequence the same mixing parameters as in case C (Table 1) but a reduced mass loss rate has been used: the parameter η was divided by 20 in order to take into account a reduction of $\dot{M}$ for low Z (Maeder 1992). The reduced mass loss rate affects only the final mass, but not the helium enrichment. These models were evolved along the RGB with effects of the He mixing on stellar structure parameter distributions fully taken into account in the stellar evolution code (Sect. 3). Sequence C' was chosen because out of the sample cases listed in Table 1 it has the highest degree of helium enrichment, in contrast to the previous, unmixed, background models. In this second set of nucleosynthesis calculations we repeat the case of the first set (Fig. 9), i.e. mixing down to $\triangle X = 0.2$ (solid lines), but also add two computer runs (dashed lines) in which the mixing was chosen to be so deep that a high enrichment in He of the envelope was guaranteed. We label these calculations by $\delta m_{\rm mix} = 0.04$, which is the penetration depth needed to mix down to $\triangle X = 0.37$.

Comparison of the results obtained in the two sets of calculations allows to draw the following conclusions:

- mass loss is practically unimportant for this study (at least within the prescriptions and variations used in the various calculations);
- making use of mixed background models instead of unmixed ones does not seriously affect the theoretical dependences of [Na/Fe] on [O/Fe] (compare the solid curves in Figs. 9 and 11); therefore the details of the mixing prescription used for the background models are not significant for the nucleosynthesis results.
- the total He enrichment of the convective envelope calculated in the post-processing way agrees very well with the final envelope He abundance obtained in the full evolutionary calculations with additional deep mixing;
- values $\triangle Y_{\rm env} > 0.15$ were obtained only in the two computer runs with the depth $\delta m_{\rm mix} = 0.04$, but in these cases additional mixing penetrated so deeply that it resulted in the [Na/Fe] on [O/Fe] dependences evidently inconsistent with the observations (dashed curves in Figs. 11 and 12).

A simple inspection of Figs. 9-12 allows the conclusion that *the global anticorrelation of [O/Fe] vs. [Na/Fe] as a whole and especially the [Na/Fe] values in its low oxygen abundance tail certainly rule out any hypothesis about an increase of more than* $\triangle Y_{\rm env} \approx 0.10$ *in the envelope He abundance of globular-cluster red giants.* A physical reason for this constraint is the above-mentioned inability of additional mixing to penetrate the second Na abundance rise lying at $\delta m \leq 0.06 \div 0.07$ as hinted by the observed global anticorrelation. In the starting models $\delta m \geq 0.07$ corresponds to $\triangle X \leq 0.05$ and, therefore, the envelope He enrichment is not expected to be much larger than $\triangle Y_{\rm env} \approx 0.05$.

5. Discussion

If the O-Na-anticorrelation observed in many globular cluster red giants is indeed due to a deep mixing process beyond the standard effects taken into account in canonical stellar evolution theory, the question is justified whether this deep mixing might affect the H-He-profile as well. In this case, consequences for the red giant evolution including phases of enhanced luminosities and mass loss could result. We have, therefore, discussed both the evolutionary and nucleosynthetic effects quantitatively by performing stellar evolution calculations including deep mixing and post-processing nucleosynthesis models (the

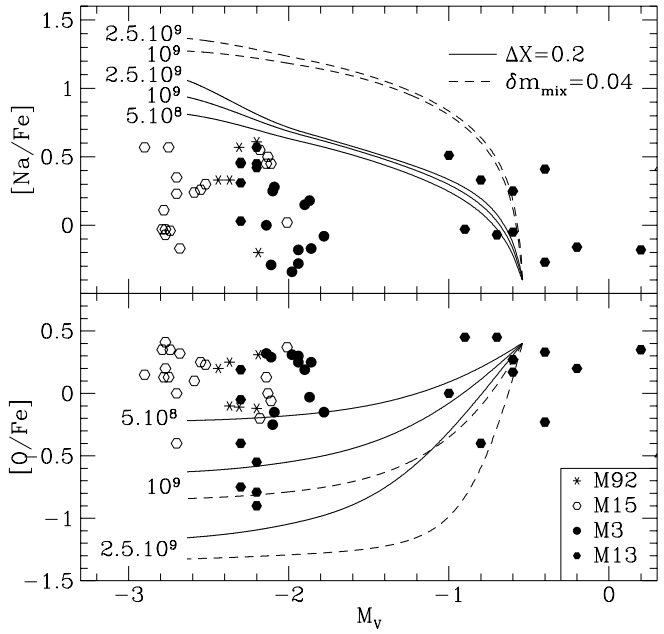

Fig. 13. [Na/Fe] and [O/Fe] for giants in globular clusters. The symbols identify individual clusters and have the same meaning as in Fig. 1. Overlaid are the five theoretical predictions shown in Fig. 11, labeled by the values of $D_{\rm mix}$. In the lower panel the two higher values relate to two lines each.

latter as we did in our earlier papers Denissenkov & Weiss 1996; Denissenkov et al. 1998).

From arguments depending only on nucleosynthesis we could already infer that for temperature profiles typical of hydrogen-burning shells mixing of appreciable amounts of helium can only be achieved if the second Na rise is penetrated. This, however, leads to oxygen and sodium anomalies exceeding those observed (with the exception of a few stars in ω Cen, a multi-metallicity, untypical cluster). In terms of our normalized mass coordinate (defined such that $\delta m = 0$ at $X = 10^{-4}$ at the bottom of the shell) this puts an observationally constrained limit for the maximum mixing depth of $\delta m_{\rm mix} > 0.06 \div 0.07$. Our complete models confirm this argument: helium enrichment in excess of $\triangle Y_{\rm env} \approx 0.05$ due to deep mixing can be ruled out for those stars with Na-O-anomalies as observed in clusters such as M15, M92, M3, and even M13 which presents one of the most extended blue horizontal branches.

The details of the surface abundance history along the RGB depend on the details of the deep mixing process and thus on its nature which we did not attempt to specify here. In particular, the field-to-cluster differences must be understood (especially the fact that field giants do not present the O-Na anticorrelation (Gratton et al. 2000), indicating a deeper and more efficient mixing in their globular cluster counterparts) and seem to point out a non-negligible impact of environmental effects on the extra mixing efficiency.

However, we can compare the observations with the histories of Na and O abundance anomalies predicted by our simple mixing prescriptions in order to get constraints for a solid physical model. This is done in Fig. 13, which shows surface abundances for several clusters as a function of brightness, i.e. progressing evolution. Also shown is the theoretical prediction of the five calculations displayed in Fig. 11. Although the observational data are very few (the uncertainty in the abundances is of order 0.2 dex), and information for stars before or at the bump is available only for M13, some effects can be recognized, nevertheless.

All clusters show the whole spread of Na abundances between the canonical case without extra mixing (they would lie on a horizontal line) and that as obtained from the calculations with less deep mixing (solid lines). As already mentioned, very low O abundances are only found in M13 giants, and the observed spread for this element is a signature of the mixing rate. For both elements the abundance anomalies are limited to values predicted by models with extra mixing *not* penetrating the second ^{23}Na rise in the hydrogen shell. Stars with intermediate anomalies we interpret as being due to mixing penetrating less deeply into the hydrogen shell. They could be reproduced with properly adjusted mixing parameters.

Over the small brightness interval for which we have data (for all the clusters except M13 only the brightest giants are accessible), no significant abundance evolution is recognizable. The increase in $[{\rm Na/Fe}]$ at the RGB tip obtained in all calculations labeled $\triangle X = 0.20$ is not visible in the observations, which may be taken as indication that the physical reasons (e.g. rotation) for the additional mixing have lost their importance or even vanished. Such a possible time dependence of the extra mixing has not been taken into account in our simple mixing prescriptions, but should result from more physically motivated models. (We recall that in Denissenkov & Weiss (1996) the carbon evolution could be reproduced with constant mixing parameters, however.) We will therefore, in a forthcoming paper, use the model by Denissenkov & Tout (2000), which includes temporal changes in the diffusion constant due to angular momentum transport.

In our models, the largest abundance changes take place at the onset of the additional mixing, i.e., early on the RGB, after the bump (around $M_V \approx -0.5$). This might be visible in the M13 data. The low brightness group has normal abundances, but above $M_V \approx -0.4$ strong anomalies already appear, reminiscent of the steep increase in the calculations mixing deeper (dashed lines). In the case of Na no further enhancement is visible (the range of values does not varies along the RGB), while O seems to get depleted further. In spite of the incomplete data at hand, the abundance anomalies seem to develop rather early and within a narrow brightness range, but then do not increase any more. This general behaviour is consistent with our theoretical predictions – though not exactly reproduced – and again points to not too deep mixing at moderate speed. The calculations with extreme helium mixing would predict the largest O depletion and Na enhancement all along the RGB; the absence of such stars can therefore not be explained with a selection effect working against the shortest lived stars at the tip of the RGB. The fact that M13 seems to show anomalies already before the bump has to be taken with care, because we compare here only with one stellar model which has a metallicity almost a factor

of 10 smaller than that appropriate for M13. At that metallicity, the bump would occur about 1 mag earlier (and our initial model is about 0.2 mag brighter than the end of the bump). We stress the fact that the present observational data do not allow a detailed comparison with the abundance evolution, but only rough qualitative statements.

Although Fig. 13 again demonstrates how the abundance evolution depends on the assumption about the additional mixing process, our calculations also show that the nucleosynthesis argument given above is valid for *all* mixing descriptions tested and therefore model-independent. From this we predict that red giants exhibiting the observed Na-O-anomalies do not have envelopes enriched in helium by much more than $\triangle Y_{\rm env} \approx 0.05$, which is comparable to the general uncertainty in our knowledge about the helium abundances in such stars.

Concerning the brightness reached during the RGB evolution, we showed that for specific mixing prescriptions large excess luminosities can be achieved at the end of the evolution without simultaneous mixing of large amounts of helium. As the reason we could identify the burning of the outer parts of the hydrogen shell where some H-He-mixing had happened in earlier phases. These regions become hot enough for significant hydrogen burning on such short time-scales that the deep mixing process is not able to mix the products any longer into the convective envelope. Such models experience very strong mass loss under the assumption of the continuing validity of a Reimers-type stellar wind and finish the RGB phase with total masses below $0.6\,M_{\odot}$ and envelope masses of only 10% of this. They could be candidates for blue HB stars and would link observed abundance anomalies, deep mixing and the second parameter problem, as suggested by Langer & Hoffman (1995) and Sweigart (1997a). They would avoid the problem of overproducing O-Na-anomalies as would result from the helium mixing investigated by Sweigart (1997a).

However, we repeat our warning that the details of the evolutionary consequences of deep mixing depend crucially on the mixing process and history. Mixing speed and depth are both important for the amount of helium mixed and for the result of the competing processes "mixing" and "burning" and their timescales. The mixing depth is also linked to the criterion for deep mixing, for which we have investigated several simple recipes.

To conclude, we need a solid physical picture for the deep mixing process in order to be able to investigate its effect on red giant evolution further. Presently, we can only point out some interesting possibilities – such as the overluminosities – and derive model-independent features, such as our main conclusion that the observed anomalies of oxygen and sodium rule out strong helium enhancement and therefore very deep mixing.

Acknowledgements. We are grateful to A. Sweigart for helpful discussions. This study was partly done while CC and PAD visited the Max-Planck-Institut für Astrophysik in Garching. They express their gratitude to the staff for hospitality and support. We appreciate the very careful work of an anonymous referee, whose detailed and constructive comments helped to improve this paper.

References

Angulo C., Arnould M., Rayet M., et al., 1999, Nucl. Phys. A 656, 3
Armosky B.J., Sneden C., Langer G.E., Kraft R.P., 1994, AJ 108, 1364
Boothroyd A.I., Sackmann I.J., 1999a, ApJ 510, 232
Boothroyd A.I., Sackmann I.J., 1999b, ApJ 510, 217
Brown J.A., Wallerstein G., 1992, AJ 104, 1818
Cavallo R., Sweigart A., Bell R., 1998, ApJ 492, 575
Charbonnel C., 1995, ApJ 453, L41
Charbonnel C., Vauclair S., Zahn J.P., 1992, A&A 255, 191
Charbonnel C., Brown J.A., Wallerstein G., 1998, A&A 332, 204
Da Costa G.S., 1998, In: Bedding T.R., Booth A.J., Bavis J. (eds.) Fundamental Stellar Properties: the interaction between observation and theory. IAU Symp. 189, Kluwer, Dordrecht, p. 193
Denissenkov P.A., Weiss A., 1996, A&A 308, 773
Denissenkov P.A., Denissenkova S.N., 1990, SvA Lett. 16, 275
Denissenkov P.A., Weiss A., Wagenhuber J., 1997, A&A 320, 115
Denissenkov P.A., Da Costa G.S., Norris J.E., Weiss A., 1998, A&A 333, 926
Denissenkov P.A., Tout C.A., 2000, MNRAS, accepted
Drake J.J., Smith V.V., Suntzeff N.B., 1992, ApJ 395, L95
Fujimoto M.Y., Aikawa M., Kato K., 1999, ApJ 519, 733
Gratton R.G., Ortolani S., 1989, A&A 211, 41
Gratton R.G., Sneden C., Carretta E., Bragaglia A., 2000, A&A 354, 169
Ivans I.I., Sneden C., Kraft R.P., et al., 1999, AJ 118, 1273
Kraft R.P., 1994, PASP 106, 553
Kraft R.P., Sneden C., Langer G.E., Prosser C.F., 1992, AJ 104, 645
Kraft R.P., Sneden C., Langer G.E., Shetrone M.D., 1993, AJ 106, 1490
Kraft R.P., Sneden C., Smith G.H., et al., 1997, AJ 113, 279
Kraft R.P., Sneden C., Smith G.H., Shetrone M.D., Fulbright J., 1998, AJ 115, 1500
Langer G.E., Hoffman R.D., Sneden C., 1993, PASP 105, 301
Langer G.E., Hoffman R.D., 1995, PASP 107, 1177
Langer G.E., Hoffman R.D., Zaidins C.S., 1997, PASP 109, 244
Maeder A., 1992, A&A 264, 105
Maeder A., Zahn J.P., 1998, A&A 334, 1000
Minniti D., Peterson R.C., Geisler D., Clarin J.J., 1996, ApJ 470, 953
Norris J.E., Costa G.S.D., 1995, ApJ 441, L81
Palacios A., Leroy F., Charbonnel C., Forestini M., 1999, preprint astro-ph/9910289
Paltoglou G., Norris J.E., 1989, ApJ 336, 185
Peterson R.C., Rood R.T., Crocker D.A., 1995, ApJ 453, 214
Pilachowski C.A., Sneden C., Kraft R.P., Langer G.E., 1996, AJ 112, 545
Powell D.C., 1999, PASP 111, 1186
Reimers D., 1975, Mem. Soc. Roy. Sci. Liège 8, 369
Shetrone M.D., 1996a, AJ 112, 1517
Shetrone M.D., 1996b, AJ 112, 2639
Smith G.H., Tout C.A., 1992, MNRAS 256, 449
Sneden C., Kraft R.P., Prosser C.F., Langer G.E., 1991, AJ 102, 2001
Sneden C., Kraft R.P., Shetrone M.D., et al., 1997, AJ 114, 1964
Sweigart A.V., 1997a, ApJ 474, L23
Sweigart A.V., 1997b, In: Philip A.G.D., Liebert J., Saffer R., Hayes D.S. (eds.) The Third Conference on Faint Blue Stars. IAU Colloq. No. 95, L. Davis Press
Sweigart A.V., Mengel K.G., 1979, ApJ 229, 624
VandenBerg D.A., Larson A.M., De Propris R., 1998, PASP 110, 98
Whitney J.H., O'Connel R.W., Wood R.T., 1994, AJ 108, 1350
Zahn J.P., 1992, A&A 265, 115
Zaidins C., Langer G.E., 1997, PASP 109, 244